Journal Name

ARTICLE TYPE

Cite this: DOI: 10.1039/xxxxxxxxxx

Demonstration of fluorescence enhancement via Bloch surface waves in all-polymer multilayer structures†

Lucia Fornasari,[a] Francesco Floris,[a] Maddalena Patrini,[a] Davide Comoretto[b] and Franco Marabelli[a]

Received Date
Accepted Date

DOI: 10.1039/xxxxxxxxxx

www.rsc.org/journalname

An all-polymer photonic structure constituted by a Distributed Bragg Reflector topped with an ultrathin fluorescent polymer film has been studied. A Bloch surface wave resonance has been exploited to improve pumping efficiency. A strongly polarization and angle dependent fluorescence signal is found with respect to the light pumping beam and the emitted wavelength. Matching the most favorable condition for the pump coupling and the collection geometry, the signal obtained from the structure appears to be two orders of magnitude larger than the one of the bare emitting film.

1 Introduction

During the last decades, photonic crystal (PhC) structures have attracted the interest of the scientific community due to their ability to control the propagation of light and the light-matter interaction. PhCs are composite materials characterized by a periodic modulation of the dielectric function on a scale comparable to the wavelength of interest, which allows for the control of light propagation including even confinement below the diffraction limit.[1] Indeed, light diffraction by all the dielectric lattice planes gives rise to constructive or destructive interference effects. When destructive interference occurs, photons are not allowed to propagate through the structure and are then back-reflected: this is the origin of the photonic band gap (PBG).[2] By changing the structure of the system, the engineering of the density of photonic states is possible. Yablonovitch, for example, proposed, in his pioneering work,[3] to exploit the PBG to inhibit the spontaneous emission of an optical emitter. To this aim, nowadays, the employment of PhC structures to suppress, enhance or redistribute the spontaneous emission of a fluorophore is still a hot topic that stimulates an intensive investigation.[4–10] In this contest, Distributed Bragg Reflectors (DBRs), i.e. planar one-dimensional (1D) multilayer structures well known since long time,[11] have been revamped when used in specific configurations such as those sustaining Bloch Surface Waves (BSWs). BSWs are surface confined modes that arise at the boundaries of a DBR to the environment and have frequency dispersion within the PBG.[12] The electromagnetic (e.m.) field confinement at the environment-PhC interface is achieved on one side owing to the PBG, which prevents light propagation inside the system and reflect it back and on the other side by total internal reflection, which is responsible for an exponential decay of the e.m. field in the external medium. The different confinement mechanisms acting for BSWs stimulated a wide range of possible applications in different fields. Indeed, some authors proposed to exploit the near-interface localization of the e.m. field via BSW to enhance the Raman scattering[13] or the diffraction power in a biosensing device[14–18] and to modify the spatial distribution of light emission from a dye.[19–21] The local field enhancement at the surface of one-dimensional photonic crystals after BSW excitation has been exploited to increase the fluorescence emission of chromophores[22] or to enhance the fluorescence detection of miRNA.[23] However, in all these works, the materials employed to realize the DBR structure are inorganic semiconductors and oxides. All-polymer DBR, in spite of

[a] Department of Physics, University of Pavia, Via Bassi 6, 27100 Pavia, Italy. E-mail: lucia.fornasari@unipv.it
[b] Department of Chemistry and Industrial Chemistry, University of Genova, via Dodecaneso 31, 16146 Genova, Italy. E-mail: davide.comoretto@unige.it

† Electronic Supplementary Information (ESI) available. See DOI: 10.1039/b000000x/

their reduced dielectric contrast, have some advantage with respect to their inorganic counterpart in terms of mechanical performances (flexibility, bendability and adaptability to preformed surfaces) and have been successfully exploited for selected applications ranging from lasing to sensing.[24–35] Moreover, industrial techniques typical of polymer world based on coextrusion (and succeeding roll-to-roll, shear or stretching) allow to produce large area (square meter) planar photonic crystal structures even more complicated than standard DBR.[36–39]

In a previous work, we suggested to exploit the BSW resonance in an all-polymer DBR to enhance the fluorescence of an optical emitter by tuning the BSW to the excitation wavelength.[40] In this work we want to optimize all-polymer photonic crystals in enhancing and redistributing in spectrum, as well as in angle, the emission of a fluorescent polymer.

2 Sample preparation and characterization techniques

Several ten-periods DBR structures were prepared by dynamic spin coating of cellulose acetate (CA) and poly(vinyl-carbazole) (PVK) solved in orthogonal solvent onto a cover glass substrate. The active medium was constituted by an ultra-thin (as derived from spectroscopic ellipsometry 3 nm) poly(9,9-dioctylfluorenyl-2,7-diyl-co-1,4-benzo-2,1'-3)-thiadiazole) (F8BT) film. To obtain pure films, the F8BT was solved in toluene and, afterward, cast on the top of the DBR structure, terminated by a CA layer. More details on the preparation can be found elsewhere.[26,40] A sketch of the final structure is reported in Figure 1. For the sake of simplicity, in the following we will refer to such a structure as DBR+F8BT.

In order to determine the films thickness and to characterize the dielectric response of each material, thin films of each polymer have been grown in the same experimental conditions on glass and silicon substrates as well as on the other polymer used in the DBR structure in order to impart the same friction properties and then to reproduce the thickness of the layer by considering the effect of different substrate surface roughness. Spectroscopic ellipsometry (SE) measurements have been performed, using a VASE instrument by J. A. Woollam Co., in the range $(250 \div 2500)$ nm at different incidence angles from 60° to 75°. In parallel, transmittance (T) at normal incidence has been measured with a Varian Cary 6000i spectrometer in the spectral range $(300 \div 1800)$ nm. As a result, the complex dielectric function $\varepsilon = \varepsilon_1 + i\varepsilon_2$ for the three materials (CA, PVK and F8BT) was evaluated by WVASE32®software, adopting oscillator models, which guarantee Kramers-Kronig consistency. In addition, from the simultaneous best-fit of SE and T spectra, the thicknesses of the polymer layers were determined. By considering all the samples produced (10 DBR and all the corresponding references), CA, PVK and F8BT thicknesses result in the range $64 \div 71$ nm, $111 \div 121$ nm and $1.7 \div 3.3$ nm, respectively. In the following, we consider a sample where CA, PVK and F8BT measure 69.4 ± 1.7 nm, 113.6 ± 1.4 nm and 2.8 ± 0.5 nm. DBRs do not need to satisfy the common quarter-wave stack condition since engineered only to support BSW mode at the laser exciting wavelength.

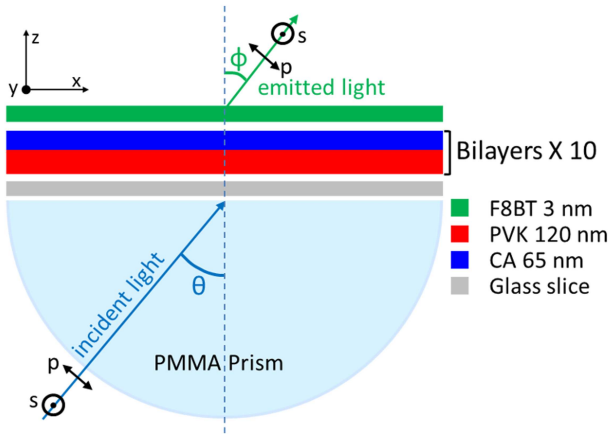

Fig. 1 Sketch of the DBR+F8BT device. A 10 PVK:CA bilayer DBR capped with F8BT is grown on a thin cover glass substrate and glued to a PMMA semi-cylinder prism.

The optical characterization of the DBR structures has been completed with attenuated total reflectance (ATR) while the response of the active medium (F8BT) has been characterized with angle-resolved photoluminescence (PL) measurements. In order to perform angle-resolved ATR and PL measurements, a poly(methyl methacrylate) (PMMA) semi-cylinder has been glued to the DBR substrates and used as a prism (see Figure 1). ATR measurements have been performed in the range $(350 \div 800)$ nm at different angles of incidence θ between 5° and 80°, with a Fourier transform infrared spectrometer (Bruker IFS66s) coupled to a home-made micro-reflectance setup. Measurements are performed with s- and p-polarization with respect to the plane of incidence, which is selected by means of a calcite Glan-Taylor polarizer. A bare PMMA prism and a glass slice glued onto a PMMA prism have been measured as references for the ATR spectra. PL measurements have been performed with a laser diode (excitation wavelength of 405 nm and power of 5 mW) impinging on the sample from the prism side. Then, the emission was collected by a lens in the front of the sample at different collection angles ϕ (lens acceptance angle of less than 5°). PL signal of the DBR+F8BT sample has been recorded as a function of the pump incident angle θ in the range $(0° \div 80°)$ and of the emission angle ϕ in the range $(0° \div 70°)$. In order to evaluate the amount of fluorescence enhancement, we considered proper reference sys-

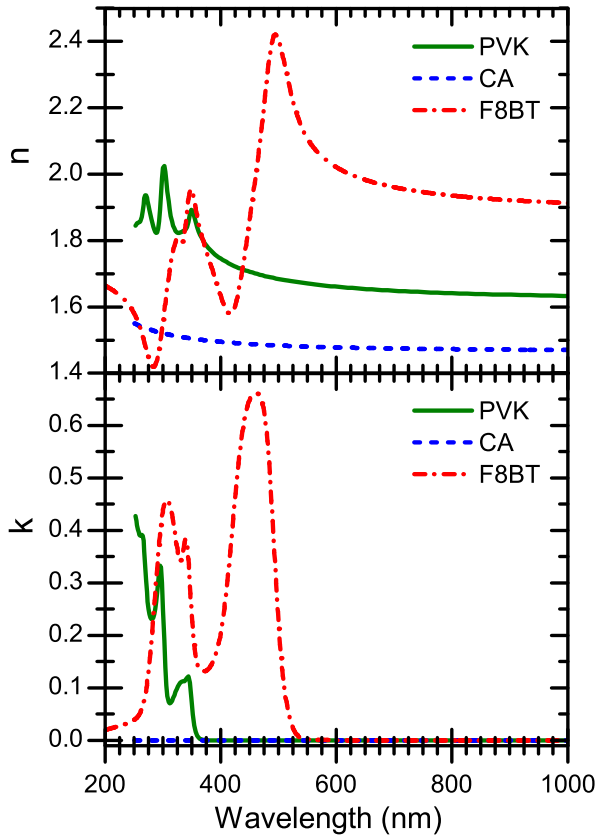

Fig. 2 Refractive index n and extinction coefficient k as determined through SE for PVK (green line), CA (blue dash line) and F8BT (red dash-dot line) thin films.

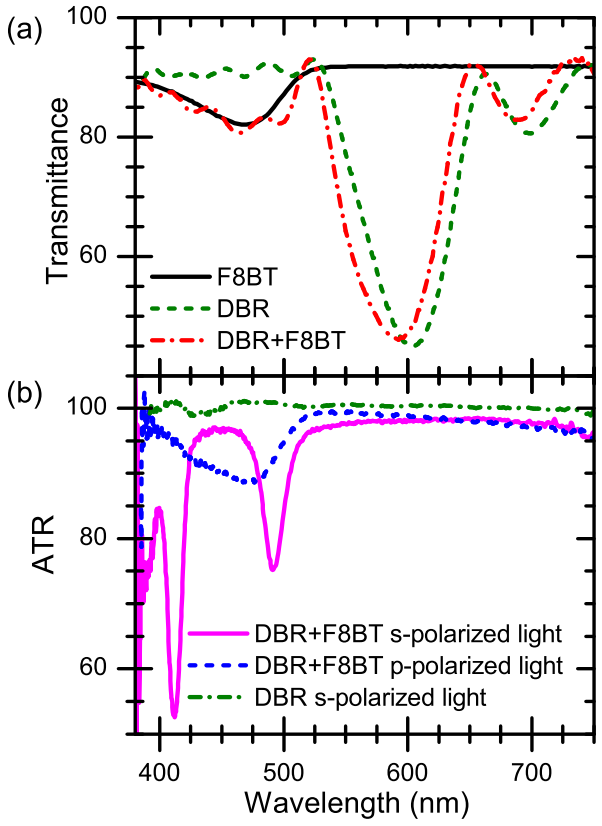

Fig. 3 (a) Comparison of the transmittance spectra of a F8BT film (black line), a bare PVK:CA DBR (green dash line), and of the DBR+F8BT structure (red dash-dot line); (b) ATR spectra at $\theta = 45°$ of the bare DBR for s-polarization (green dash-dot line) and of the DBR+F8BT system for both s- and p-polarization (magenta line and blue dash line, respectively).

tems, i.e. a F8BT film cast on a CA layer on a glass substrate either free or glued to a PMMA prism. The F8BT thickness for the reference is 3.3 ± 0.03 nm. We want to highlight that, in all the presented ATR and PL experiments the samples are glued on a PMMA prism. Theoretical calculations of the PBG and BSW dispersion and of the electric field distribution have been performed by the transfer matrix method.

3 Results and discussion

Figure 2 shows the refractive index and the extinction coefficient for the investigated materials in the range $(200 \div 1000)$ nm. CA and PVK films are transparent in the visible and near-infrared and have a different refractive index ($n_{PVK} = 1.64$ and $n_{CA} = 1.47$ at 1000 nm), as expected.[25,28,40,41] CA remains transparent in all the investigated range while PVK shows the well-known absorption bands due to the aromatic side groups below 400 nm.[42] The absorption properties of F8BT are in agreement with previous findings[43–45] with the main broad and structureless absorption at 480 nm. The refractive index spectrum reveals features corresponding to those of the extinction coefficient and a value in the transparency region of about 1.9@1000 nm.

Figure 3(a) reports the normal incidence T spectra for a F8BT film, a PVK:CA DBR and for the DBR+F8BT structure. F8BT film transmittance is high except for a broad structureless absorption band (between 400 and 500 nm), T of the DBR is characterized by a strong minimum in correspondence of the 1^{st} order PBG feature, which has been tuned at 600 nm with a linewidth of about 80 nm. Next to this prominent feature, some interference fringes appear in the spectrum due to the DBR finite size and to the refractive index contrast between the latter and the substrate. When the F8BT is cast on top of DBR, T spectrum exhibits the main features of both the constituents (red dash-dot line): the absorption band of the F8BT is modulated by the interference fringes of the DBR response, while the DBR PBG feature appears almost unchanged. The slight shift of the stop band feature as well as the small linewidth change is due to the presence of the F8BT cap-

ping layer. The ATR spectra of the DBR+F8BT structure, either p- or s- polarized, for $\theta = 45^\circ$ are also shown for comparison in Figure 3(b). It's worthwhile noticing that the ATR of the bare DBR (also shown in Figure 3(b)) exhibits the same response of the bare PMMA prism, that is a 100% reflectance (R), with no absorption signature. When the F8BT is cast on the top of the DBR and R is measured above the critical angle (which is about 42° in air), p-polarized response just shows the effect of the F8BT absorption and it is fully comparable with T results reported in Figure 3(a). For s-polarized probing light, a totally different situation occurs: two very intense absorption-like features appear in the spectrum at 410 and 490 nm, much narrower than the PBG and F8BT absorption band. Since the only optical effect introduced with respect to the bare DBR is the absorption of F8BT, these features deserve a more detailed analysis being not simply related to the absorption spectrum of the conjugated polymer.

Figure 4(a) and (b) show the complete R and ATR characterization of the DBR+F8BT structure for s- and p-polarization, respectively. Below the critical angle and for both light polarizations, R spectra highlight the dispersion of the 1^{st} order PBG feature as a function of the angle of incidence in agreement with previous findings.[26] No signature is present of the F8BT capping layer. Above the critical angle, the ATR regime is achieved and a dramatic difference between p- and s-light polarization can be observed. When the incident light is p-polarized, the ATR signal is dominated by the total reflection with a slight decrease in the range $(400 \div 500)$ nm due to the absorption of the F8BT capping layer. In the case of s-polarized incident light, two absorption-like features appear in the spectra, exhibiting dispersion behavior with increasing θ. One is in the range $(450 \div 500)$ nm, where also F8BT absorption occurs. This structure is likely to be due to an interplay between the absorption of the F8BT, which would lower the ATR signal (as in the case of p-polarized incident light) and the onset (the low energy edge) of the DBR PBG feature (which prevents light propagation through the system, thus increasing the average R value). Very interesting to us is the second structure occurring in the range $(400 \div 450)$ nm. It is relatively narrow and appears very close to the high energy edge of the PBG, but within the PBG. Moreover, this structure shows a clear dispersion with the angle of incidence. Instead, such a feature does not occur in p-polarized spectra. This higher energy feature appearing in the ATR spectra with s-polarized incident light can be interpreted as a BSW running through the last layer of the capped DBR system.[40] The BSW mode can be excited only with s-polarization and when a proper energy-wavevector matching is attained. Panel (c) and (d) report the R and ATR spectra, calculated with the WVASE32®software, using the materials optical functions and thicknesses derived by the best-fit on SE and T data. The calculated spectra (lower panels) well reproduce all the spectral features and the overall intensities of the experimental data

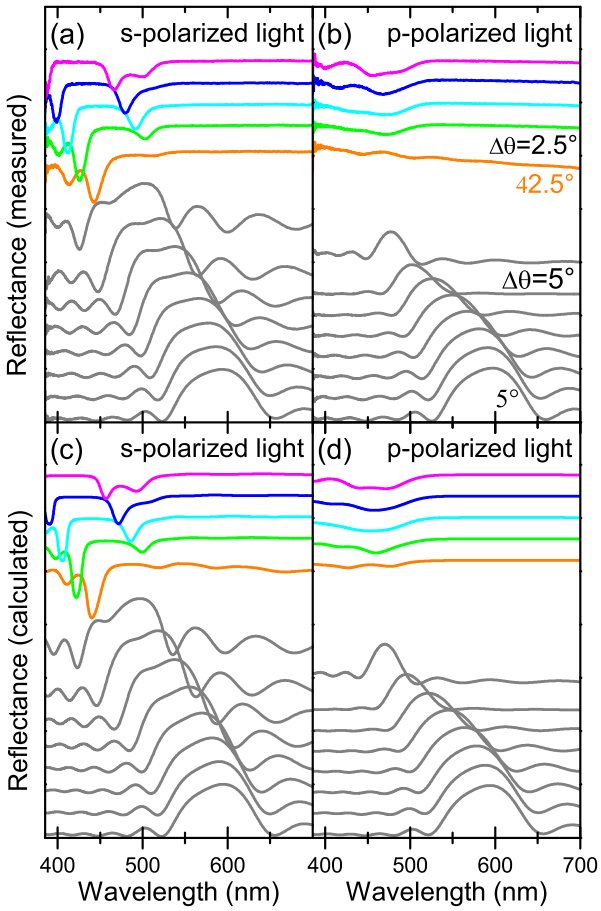

Fig. 4 Reflectance spectra of the DBR+F8BT structure glued on a PMMA prism as a function of the external incidence angle θ. Grey lines are for the standard reflectance regime, while colored lines are for the ATR regime above the critical angle. The (a) and (b) panels show spectra measured with s- and p-polarized light, respectively. The (c) and (d) panels show the spectra calculated with the WVASE32®software using the materials parameters (thicknesses and optical functions) obtained from the best-fit to SE and T data. In all panels the spectra are vertically displaced for clarity with $\Delta R = 0.2$.

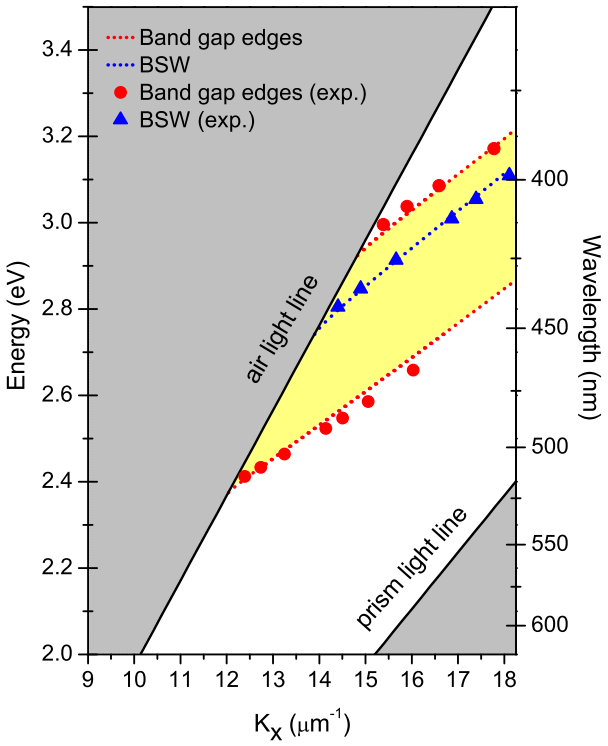

Fig. 5 PBG (red dots) and BSW mode (blue triangles) dispersion extracted from the experimental data reported in Figure 4(a). The corresponding dispersions, as calculated for s-polarized light, are shown as dot lines.

(upper panels).

In order to better identify the various structures of the ATR spectra we have calculated the photonic modes supported by the structure through a transfer matrix method. Both PBG and BSW dispersion for s-polarized light are shown in Figure 5 together with the experimental data extracted from the ATR spectra (Figure 4(a)). The BSW dispersion relation is clearly visible inside the PBG, delimited by the two band edges, and, as expected, it is in excellent agreement with the theoretical curve. In addition, to highlight the property of the BSW we have simulated, within the same theoretical model, the spatial localization of the BSW excited in the DBR+F8BT structure with a light source at 405 nm wavelength impinging on the sample at $\theta = 47°$ (the angle for which the ATR structure is observed at 405 nm). The result is shown in Figure 6. In this condition the e.m. field is localized on top of the structure. The relatively low field localization close to the surface is due to the finite size of the DBR. In the case this

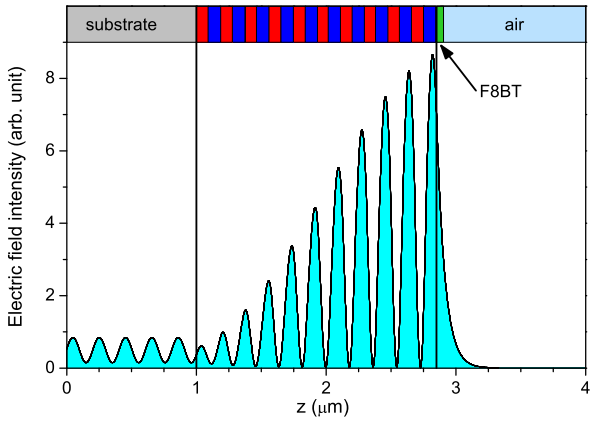

Fig. 6 Electric field intensity distribution as calculated for a light wavelength of 405 nm impinging in ATR configuration on the DBR+F8BT structure with $\theta = 47°$. A sketch of the system depth profile is also shown.

momentum-energy matching condition is not achieved, the electric field distribution is centered inside the PhC (see ESI Figure 1). The surface localization of the BSW is the clear indication of its great interest for sensing since it probes mainly the surface of the sample, which is directly in contact with the environment.

As a further step, we have exploited the BSW field localization to enhance the optical pump efficiency in a fluorescence experiment. We measured the PL spectrum of the DBR+F8BT structure excited by a laser beam at 405 nm with variable angle of incidence θ, for both s- and p-input polarizations. In Figure 7(a) and (b), we plot the PL intensity emitted by the DBR+F8BT structure as a function of both the emission wavelength and the laser beam incidence angle for s- and p-polarization (emitted light is unpolarized). In the case of p-polarization (Figure 7(b)), the PL intensity decreases in a non-uniform way by increasing θ. The emission reaches a minimum at about 40°; then, a rapid PL increase occurs above the critical angle, with a local maximum around 50° followed by a series of oscillations. In the case of s-polarized laser beam (Figure 7(a)), the PL intensity has a steep increase up to about 42° (the critical angle for total reflection). Then, it continues to increase, reaching a maximum at 47°. For larger angles the intensity rapidly decreases to almost zero. Then, at about 70°, the signal grows again and oscillates around low intensity values. These data can be partially interpreted by considering the behavior of R of the system at the laser wavelength. When light is p-polarized R has a minimum at about $\theta = 35°$ and then reaches the ATR value. Anyway, R is lower than 100%, due to absorption effects, and is slightly modulated due to the interference in the DBR structure, which causes constructive or destructive interference fringes. When light is s-polarized, R grows till 40°, than has a plateau value and a sharp minimum at $\theta = 47°$. This

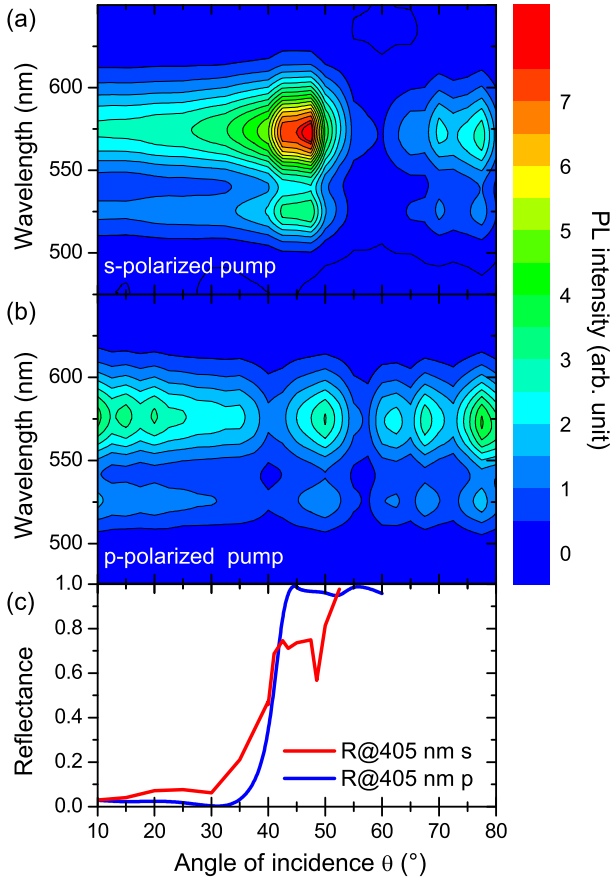

Fig. 7 (a) and (b): Contour plots of the PL spectrum intensity for the DBR+F8BT structure as a function of the pump incidence angle for s- and p-polarized laser beam, respectively. (c) Behavior of the s- and p-polarized reflectance signal collected at the pump laser wavelength (405 nm) as a function of the angle of incidence θ.

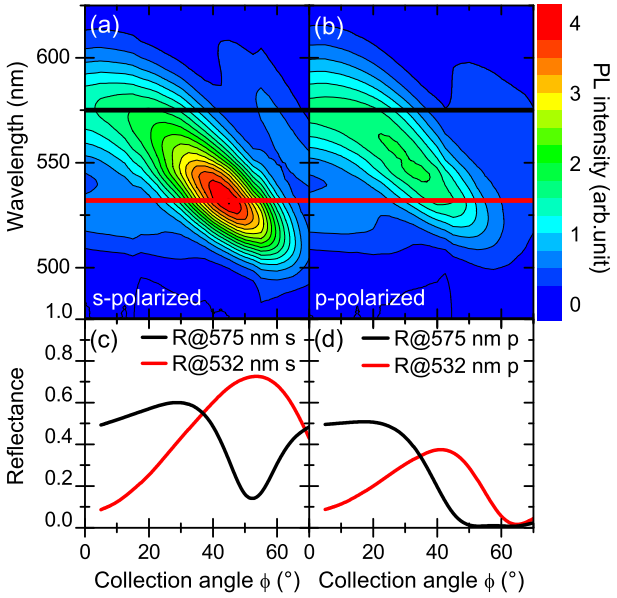

Fig. 8 (a) and (b): s- and p-polarized PL emission of the DBR+F8BT structure as a function of the wavelength and of collection angle. (c) and (d): behavior of the reflectance signal collected at 575 nm (black lines), corresponding to the wavelength of the maximum PL signal at 0°, and at 532 nm (red lines), corresponding to the wavelength of the absolute maximum PL signal, in the s-polarized case.

minimum corresponds to the excitation of the BSW (at the laser wavelength) localized at the surface of the structure. Notice that for this angle the maximum PL intensity is observed as reported in Figure 7(a). This result clearly shows that the fluorescence enhancement is directly related to the excitation of the BSW mode and then to an improvement of the absorption efficiency of the F8BT layer.

Moreover, PL spectral intensity has been also measured as a function of the collection angle ϕ, by setting the excitation laser fixed at $\theta = 47^\circ$, s-polarized, in order to maximize the pumping efficiency in the system. The corresponding data are shown in Figure 8. For both p- and s-polarized excitation, the maximum of the PL intensity spectrally blue-shifts when moving towards higher emission angles. Similar shifts can hardly be assigned to the change of the photophysical properties of F8BT and then are attributed to the photonic structure. The maximum of the emission intensity is at 45° and 30° in the s- and p-polarized case, respectively. The dispersion of PL emission approximately follows the dispersion of the DBR PBG.

In order to verify and quantify this hypothesis, we have reported in Figure 8(c) and (d) the behavior of R vs the collection angle ϕ at two wavelengths of interest: $\lambda = 575$ nm, corresponding to the wavelength of the PL maximum at $\theta = 0^\circ$, and $\lambda = 532$ nm, corresponding to the wavelength of the absolute maximum

PL signal, in the s-polarized case, occurring at 45° (panels (c) and (d) for s- and p-polarized light, respectively). At near-normal emission, the R value at 575 nm is higher than that at 532 nm. At higher emission angles the R at 575 nm falls, while that at 532 nm grows. The trend of the R should partially explain the PL features: the maximum of the PL signal follows the PBG maximum in the R. This is not surprising because light emitted inside the structure is selectively reflected by the DBR structure. Nevertheless, this qualitative explanation of the spectral shape trends is not sufficient to explain the quantitative emission enhancement. When the emission is p-polarized, the intensity of the maximum at 0° is comparable to that of the maximum at 30°, as we expect from the R values. Instead, for s-polarized light the maxima at 0° and 45° are not-comparable, there being a factor of almost 3 between the PL intensity values, not consistent with an almost similar R. Then, a further enhancement occurs and spectra cannot be interpreted just as a modal redistribution by the DBR. As a matter of fact, such an effect can be put into better evidence by analyzing in a more detail the angular distribution of the intensities, as depicted in Figure 9.

Figure 9(a) shows the emission spectra measured at different collection angles for the bare F8BT film cast onto a single CA layer on a glass slide. The highest PL intensities for the bare F8BT film are obtained by impinging with the laser pump, through the prism, at an angle close to the critical one. This angular behavior is in full agreement with previous findings reported in literature[21,40]. Here we fixed the incidence angle $\theta = 47°$, the same used for the DBR+F8BT structure. The PL intensity monotonically decreases as the emission angle increases (panel (a)), but it is always significantly lower than the PL intensity from the DBR+F8BT structure (panels (b) and (c), notice that the intensity scale is 5 times higher than in panel (a)). It is worthwhile noticing that the presence of the DBR dramatically affects the spectral shape of the PL. For the bare film PL maximum occurs around $\lambda = 540$ nm while for the DBR+F8BT structure it occurs at $\lambda = 570$ nm. Also the PL linewidth is different, being sharper when the F8BT is cast on the top of the DBR. As highlighted before, such a spectral shape modification can be qualitatively ascribed to the spectrally selective R of the DBR. For the p-polarization this roughly accounts also quantitatively for the spectral evolution. This is not the case for s-polarization, where an enhancement of 5 times in intensity is observed passing from 0° to 45°. In the polar plots we have reported the trends of the maximum intensity (black line) and of the integrated intensity (red line) as a function of the emission angle. The integrated intensity in all the plots has been normalized to the maximum value (indicated as 1), as obtained in the DBR+F8BT structure at 40° emission angle and s-polarization.

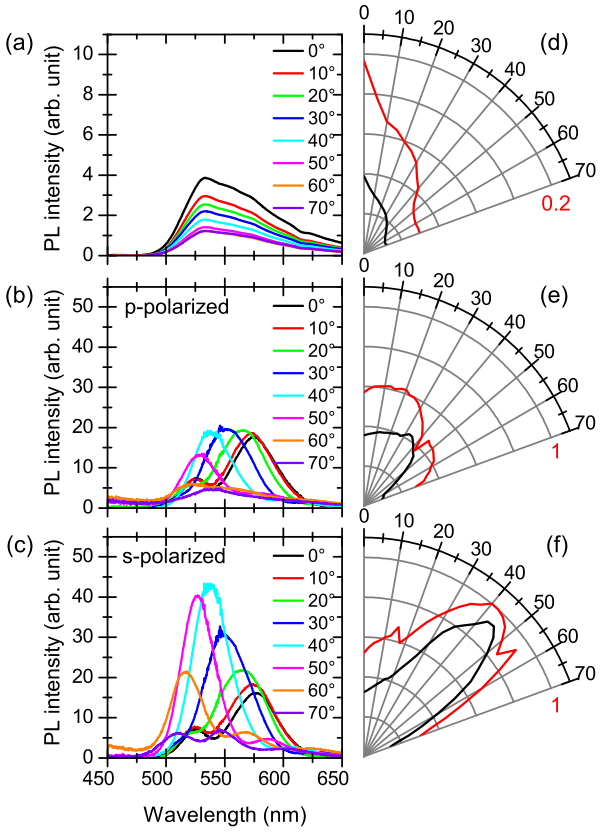

Fig. 9 PL spectra at different collection angles and polar plot of the PL maximum intensity (black line) and of the integrated intensity (red line) for: (a), (d) the un-polarized emission of a reference F8BT film; (b), (e) and (c), (f): p- and s-polarized emission of the DBR+F8BT structure. Note that the scales in panels (a) and (d) are 5 times lower than the corresponding ones of panels (b) (and (c)) and (e) (and (f)), respectively.

4 Conclusions

In the present work, we have deeply investigated the fluorescence enhancement effect achieved in an all-polymer 1D-PhC capped with an ultrathin F8BT layer. The ATR and PL spectra of our system clearly highlight a strongly polarization dependent behavior in the interaction between input light source and PhC structure emission. When light is p-polarized, the ATR spectra show the absorption of the fluorophore on the top of the structure. Instead, in s-polarized ATR response, different spectral features can be evidenced, assigned to the effect of BSW field spatially confined at the PhC surface. Fluorescence experiments demonstrate that a significant PL enhancement can be achieved when the pumping source is resonant in energy and wavevector to the BSW photonic mode. A further enhancement can be observed when the angular distribution of the emission is also considered. The maximum in-

tensity observed at the emission angle of 45° results to be more than 10 times larger than the emission of the same F8BT film measured in the best conditions of excitation through a prism, which is, in turn almost a factor of 3 greater than that measured without prism. An even larger enhancement factor could be calculated when considering the whole amount of emitted light integrated over the solid angle (see ESI Figure 2). Measurements with an integrating sphere are planned to verify this result. Then, it is not clear whether this huge enhancement factor can be ascribed only to the increase of pump efficiency or also to an improved emission efficiency, induced by the large photonic density of states supplied by DBR. In order to investigate this point, time resolved emission measurements should be performed. It is worthwhile noticing that these results have been obtained in an all-polymer structure produced through low-cost materials and growth technique and using a very simple optical setup. The results are thus particularly significant since can be easily transferred to large scale for sensing applications where weak PL signals or strong PL quenching effects are involved.

5 Acknowledgments

Work in Genova has been funded by the Italian Ministry of the University, Research and Instruction thorough the Progetti di Ricerca di Rilevante Interesse Nazionale 2010-2011 Program (Materiali Polimerici Nanostrutturati con strutture molecolari e cristalline mirate, per tecnologie avanzate e per l'ambiente, 2010XLLNM3). The work has been partially supported by Cariplo Foundation under the Project PHOENICS (No. 2009-2461). We thank Marco Liscidini for theoretical calculations. D.C. thanks G. Canazza for technical assistance in sample preparation.

References

1 J. D. Joannopoulos, S. G. Johnson, J. N. Winn and R. D. Meade, *Photonic crystals: molding the flow of light*, Princeton University Press, 2011.

2 M. Liscidini and L. C. Andreani, *Organic and Hybrid Photonic Crystals*, Springer International Publishing Switzerland, 2015.

3 E. Yablonovitch, *Physical Review Letters*, 1987, **58**, 2059 – 2062.

4 P. Lodahl, A. F. van Driel, I. S. Nikolaev, A. Irman, K. Overgaag, D. Vanmaekelbergh and W. L. Vos, *Nature*, 2004, **430**, 654–657.

5 M. Barth, A. Gruber and F. Cichos, *Physical Review B*, 2005, **72**, 085129.

6 L. Berti, M. Cucini, F. Di Stasio, D. Comoretto, M. Galli, F. Marabelli, N. Manfredi, C. Marinzi and A. Abbotto, *Journal of Physical Chemistry C*, 2010, **114**, 2403–2413.

7 N. Ganesh, W. Zhang, P. C. Mathias, E. Chow, J. Soares, V. Malyarchuk, A. D. Smith and B. T. Cunningham, *Nature Nanotechnology*, 2007, **2**, 515–520.

8 V. Boiko, G. Dovbeshko, L. Dolgov, V. Kiisk, I. Sildos, A. Loot and V. Gorelik, *Nanoscale Research Letters*, 2015, **10**, 1–7.

9 J.-F. Dechezelles, T. Aubert, F. Grasset, S. Cordier, C. Barthou, C. Schwob, A. Maitre, R. A. L. Vallee, H. Cramail and S. Ravaine, *Phys. Chem. Chem. Phys.*, 2010, **12**, 11993–11999.

10 W. Wang, H. Song, X. Bai, Q. Liu and Y. Zhu, *Phys. Chem. Chem. Phys.*, 2011, **13**, 18023 – 18030.

11 P. Yeh, A. Yariv and C.-S. Hong, *Journal of the Optical Society of America*, 1977, **67**, 423–438.

12 P. Yeh, A. Yariv and A. Y. Cho, *Applied Physics Letters*, 1978, **32**, 104–105.

13 S. Pirotta, X. Xu, A. Delfan, S. Mysore, S. Maiti, G. Dacarro, M. Patrini, M. Galli, G. Guizzetti, D. Bajoni *et al.*, *Journal of Physical Chemistry C*, 2013, **117**, 6821–6825.

14 M. Liscidini, M. Galli, M. Patrini, R. W. Loo, M. C. Goh, C. Ricciardi, F. Giorgis and J. Sipe, *Applied Physics Letters*, 2009, **94**, 43117.

15 M. Liscidini and J. Sipe, *Applied Physics Letters*, 2007, **91**, 253125.

16 M. Liscidini and J. Sipe, *Journal of the Optical Society of America B*, 2009, **26**, 279–289.

17 M. Shinn and W. Robertson, *Sensors and Actuators B: Chemical*, 2005, **105**, 360–364.

18 V. N. Konopsky, and E. V. Alieva, *Analytical Chemistry*, 2007, **79**, 4729–4735.

19 M. Liscidini, M. Galli, M. Shi, G. Dacarro, M. Patrini, D. Bajoni and J. Sipe, *Optics Letters*, 2009, **34**, 2318–2320.

20 R. Badugu, K. Nowaczyk, E. Descrovi and J. R. Lakowicz, *Analytical Biochemistry*, 2013, **442**, 83–96.

21 M. Ballarini, F. Frascella, F. Michelotti, G. Digregorio, P. Rivolo, V. Paeder, V. Musi, F. Giorgis and E. Descrovi, *Applied Physics Letters*, 2011, **99**, 043302.

22 I. Soboleva, E. Descrovi, C. Summonte, A. Fedyanin and F. Giorgis, *Applied Physics Letters*, 2009, **94**, 231122.

23 F. Frascella, S. Ricciardi, L. Pasquardini, C. Potrich, A. Angelini, A. Chiadò, C. Pederzolli, N. De Leo, P. Rivolo, C. F. Pirri *et al.*, *Analyst*, 2015, **140**, 5459–5463.

24 *Organic and Hybrid Photonic Crystals*, ed. D. Comoretto, Springer International Publishing Switzerland, 2015.

25 L. Frezza, M. Patrini, M. Liscidini and D. Comoretto, *Journal of Physical Chemistry C*, 2011, **115**, 19939–19946.

26 G. Canazza, F. Scotognella, G. Lanzani, S. De Silvestri, M. Zavelani-Rossi and D. Comoretto, *Laser Physics Letters*, 2014, **11**, 035804.

27 P. Lova, G. Manfredi, L. Boarino, A. Comite, M. Laus, M. Patrini, F. Marabelli, C. Soci and D. Comoretto, *ACS Photonics*, 2015, **2**, 537–543.

28 S. Gazzo, G. Manfredi, R. Pötzsch, Q. Wei, M. Alloisio, B. Voit

and D. Comoretto, *Journal of Polymer Science Part B: Polymer Physics*, 2016, **54**, 73–80.

29 C. Toccafondi, L. Occhi, O. Cavalleri, A. Penco, R. Castagna, A. Bianco, C. Bertarelli, D. Comoretto and M. Canepa, *Journal of Materials Chemistry C*, 2014, **2**, 4692–4698.

30 L. M. Goldenberg, V. Lisinetskii and S. Schrader, *Applied Physics B*, 2015, **120**, 271–277.

31 N. Valappil, M. Luberto, V. Menon, I. Zeylikovich, T. Gayen, J. Franco, B. Das and R. Alfano, *Photonics and Nanostructures-Fundamentals and Applications*, 2007, **5**, 184–188.

32 V. Menon, M. Luberto, N. Valappil and S. Chatterjee, *Optics Express*, 2008, **16**, 19535–19540.

33 T. Komikado, A. Inoue, K. Masuda, T. Ando and S. Umegaki, *Thin Solid Films*, 2007, **515**, 3887–3892.

34 R. Yagi, H. Katae, Y. Kuwahara, S.-N. Kim, T. Ogata and S. Kurihara, *Polymer*, 2014, **55**, 1120 – 1127.

35 M. Moritsugu, T. Ishikawa, T. Kawata, T. Ogata, Y. Kuwahara and S. Kurihara, *Macromolecular Rapid Communications*, 2011, **32**, 1546 – 1550.

36 C. E. Finlayson and J. J. Baumberg, *Polymer International*, 2013, **62**, 1403–1407.

37 G. Mao, J. Andrews, M. Crescimanno, K. D. Singer, E. Baer, A. Hiltner, H. Song and B. Shakya, *Opt. Mater. Express*, 2011, **1**, 108–114.

38 H. Song, K. Singer, J. Lott, Y. Wu, J. Zhou, J. Andrews, E. Baer, A. Hiltner and C. Weder, *J. Mater. Chem.*, 2009, **19**, 7520–7524.

39 http://www.toray.com/, Last accessed: 2016-02-19.

40 L. Fornasari, F. Floris, M. Patrini, G. Canazza, G. Guizzetti, D. Comoretto and F. Marabelli, *Applied Physics Letters*, 2014, **105**, 053303.

41 M. Campoy-Quiles, J. Nelson, P. Etchegoin, D. Bradley, V. Zhokhavets, G. Gobsch, H. Vaughan, A. Monkman, O. Ingänas, N.-K. Persson *et al.*, *Physica Status Solidi C*, 2008, **5**, 1270–1273.

42 D. Comoretto, G. Dellepiane, C. Cuniberti, L. Rossi, A. Borghesi and J. Le Moigne, *Phys. Rev. B*, 1996, **53**, 15653–15659.

43 M. Campoy-Quiles, G. Heliotis, R. Xia, M. Ariu, M. Pintani, P. Etchegoin and D. D. Bradley, *Advanced Functional Materials*, 2005, **15**, 925–933.

44 C. M. Ramsdale and N. C. Greenham, *Advanced Materials*, 2002, **14**, 212–215.

45 M. Tammer, L. Horsburgh, A. P. Monkman, W. Brown and H. D. Burrows, *Advanced Functional Materials*, 2002, **12**, 447–454.